doi:10.1038/nature10802

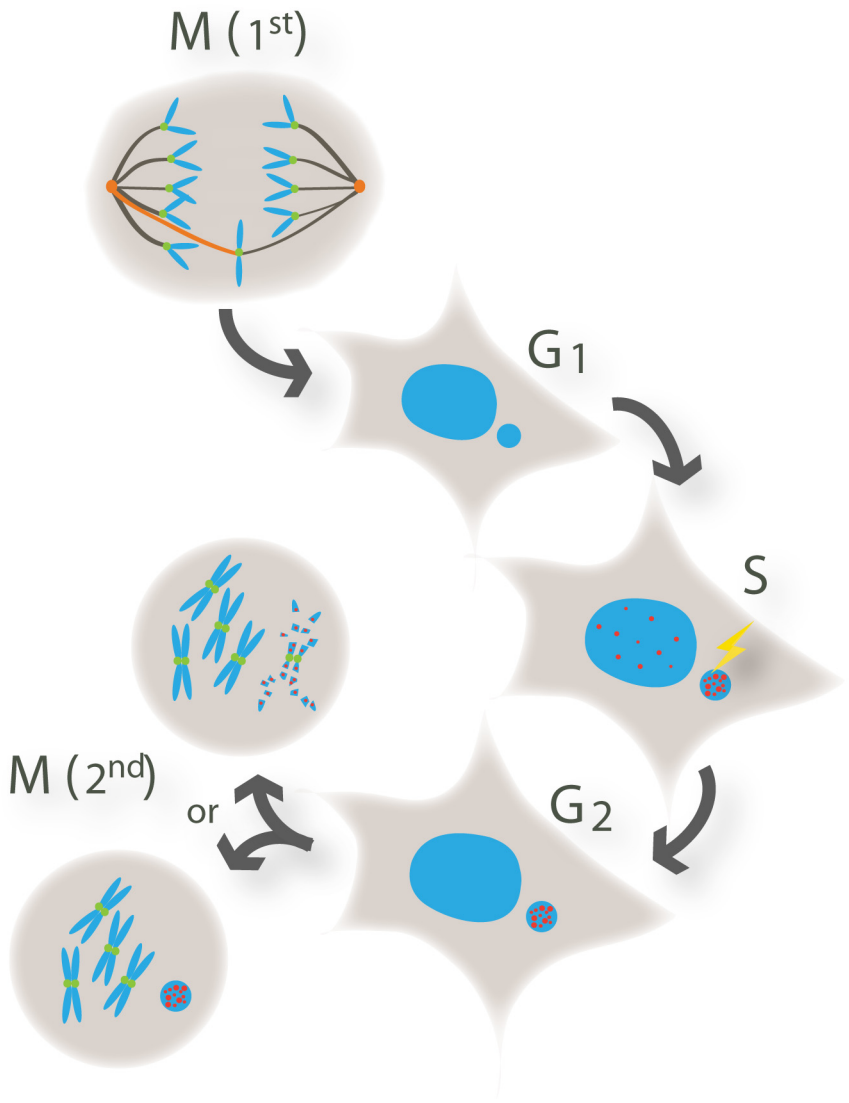

Supplementary Figure 1. A model for the development of DNA damage from mitotic chromosome segregation errors. Defects in mitosis, often originating from centrosome amplification, lead to incorrect kinetochore-microtubule attachments. This results in chromosomes that "lag" at anaphase – M(1st). Although many lagging chromosomes will be segregated correctly, lagging chromosomes that are not corrected will be partitioned into a micronucleus in the next G_1 phase of the cell cycle (G_1). In part due to defective nuclear import into micronuclei, micronuclei undergo aberrant DNA replication (S). DNA replication is not only inefficient in micronuclei, but also asynchronous with the main nucleus. This results in persistent DNA replication (delayed de novo synthesis or continued repair synthesis) that can be visualized in G_2 cells (G_2). The aberrant DNA replication can have two outcomes. First, it can produce DNA damage and mutagenesis as with any DNA replication defect, without gross alteration of the structure of the chromosome – M(2nd) bottom arrow. Second, it can produce chromosome pulverization by means of premature chromosome compaction if the cell enters mitosis while there is ongoing replication within the micronuclei -M(2nd) top arrow. Micronuclei can persist as distinct structures over several generations or the chromosome in the micronucleus can be distributed after mitosis to daughter cells.

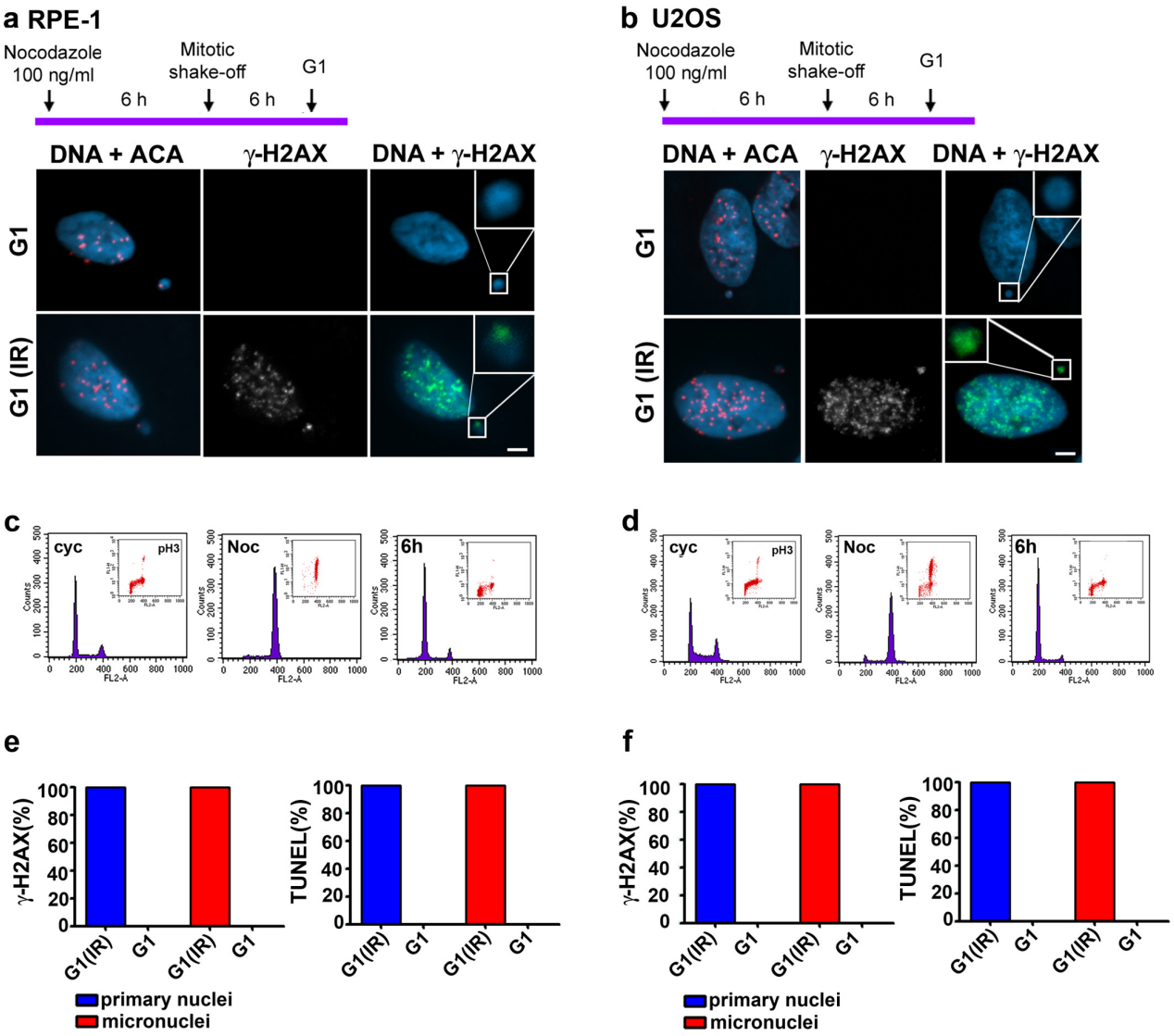

Supplementary Figure 2 (Related to Figure 1). Micronuclei do not exhibit detectable DNA damage in the G_1 phase. a,b, Top: Schematic representation of the experiment for (**a**) RPE-1 cells and (**b**) U2OS cells. **Bottom:** Representative images of (**a**) RPE-1 and (**b**) U2OS cells at the 6 h (G_1) timepoint, labelled to detect DNA (Hoechst 33342, blue), kinetochores (ACA, red) and DNA damage (γ-H2AX, green). 10 Gy irradiation (IR) is shown as a positive control. Insets show enlarged images of MN. Scale bar, 10 μm. **c, d,** FACS profiles of (**c**) RPE-1 cells and (**d**) U2OS cells at the indicated timepoints. Phospho-histone H3 (Ser 10) expression as a function of DNA content is shown in insets. **e, f**, From the G_1 population of cells, the percentage of primary nuclei (blue bars) and centric (ACA positive) MN (red bars) labelled for **(Left)** γ-H2AX and **(Right)** TUNEL from (**e**) RPE-1 cells and (**f**) U2OS cells.

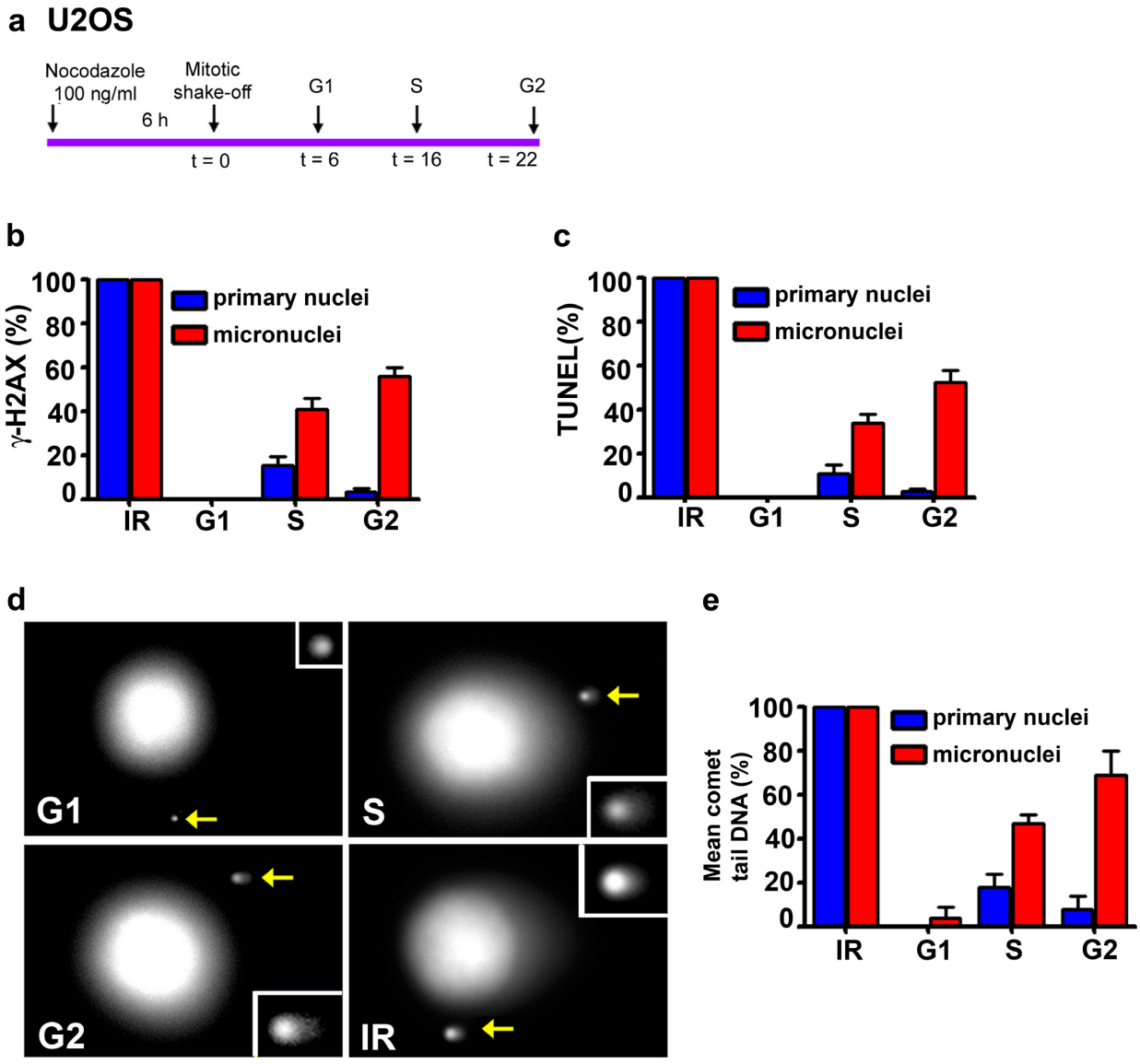

Supplementary Figure 3 (Related to Figure 1). Micronuclei develop DNA breaks in S phase. a, Schematic representation of the experiment for U2OS cells. **b,c**,The percentage of primary nuclei (blue bars) and centric (ACA positive) MN (red bars) labeled for **(b)** γ-H2AX and **(c)** TUNEL at indicated cell cycle stages. Data represents means of three independent experiments, n=100. Error bars, s.e.m. 10 Gy IR is the positive control. **d,** Representative images of comet assays from cells at the indicated cell cyle stages. Arrows indicate MN; insets show enlarged versions of MN. **e,** Comparison of mean comet tail DNA (percentage of IR control, mean of two independent experiments) in primary nuclei (blue bars) and MN (red bars) using synchronized cells as in **(a)**; n=50 cells for each sample. Error bars, s.e.m.

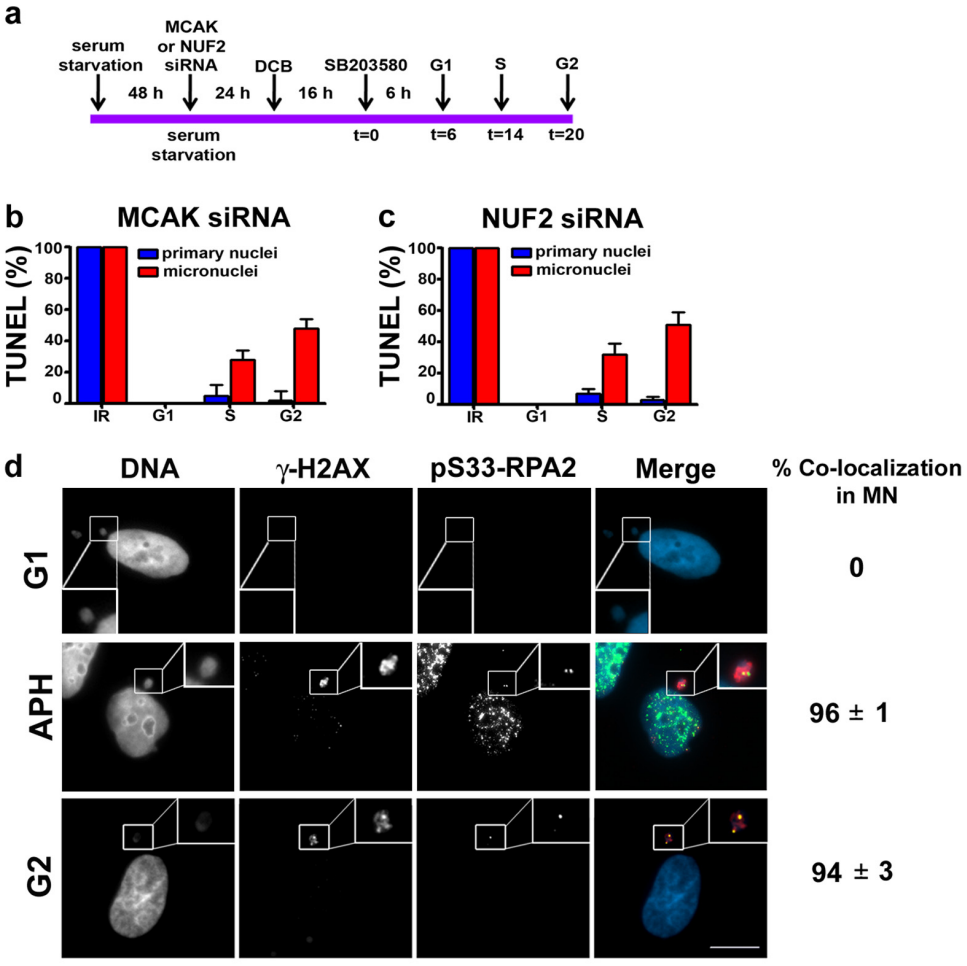

Supplementary Figure 4 (Related to Figures 1-3). Newly generated micronuclei acquire DNA breaks in S-phase that persist into G_2 irrespective of the method used to generate micronuclei. **a,** Schematic representation of the experiments. Briefly, U2OS cells were subjected to serum starvation and either MCAK[46] or NUF2[47] siRNA used. Cells were then treated with dihydrocytochalasin B (DCB) which arrests cells at G_1. To allow re-entry into the cell cycle, cells were treated with the p38 inhibitor SB203580. Cells were then collected at indicated timepoints. **b,c,** Percentages of primary nuclei (blue bars) and centric MN (red bars) with TUNEL labelling at the indicated cell cycle stages from experiments where merotely was induced by **(b)** MCAK knockdown and detached kinetochores was induced by **(c)** Nuf2 knockdown. Results represent the means of three independent experiments ± SEM, n=100. **d,** Micronuclei in G_2 cells display evidence of DNA replication stress, labelling with an antibody to detect pS33-RPA2[48]. Representative images of G_1, aphidicolin-treated (APH; 0.4 μM) and G_2 U2OS cells stained to detect RPA2 phosphorylated on Ser33 and co-labelled for γ-H2AX. Cells were synchronized as in **Supplementary Fig. 3**. The percentage of γ-H2AX positive MN co-labelled to detect pS33-RPA2 is shown (n=100). Two independent experiments were performed. Scale bar, 10 μM.

References:

(46) Kline-Smith, S. L., Khodjakov, A., Hergert, P. & Walczak, C. E. Depletion of centromeric MCAK leads to chromosome congression and segregation defects due to improper kinetochore attachments. Mol Biol Cell 15, 1146-1159 (2004).
(47) DeLuca, J. G., Moree, B., Hickey, J. M., Kilmartin, J. V. & Salmon, E. D. hNuf2 inhibition blocks stable kinetochore-microtubule attachment and induces mitotic cell death in HeLa cells. J Cell Biol 159, 549-555 (2002).
(48) Vassin, V.M. , Anantha, R.W., Sokolova, E., Kanner, S. & Borowiec, J.A. Human RPA phosphorylation by ATR stimulates DNA synthesis and prevents ssDNA accumulation during DNA-replication stress. J Cell Sci 122, 4070-4080 (2009).

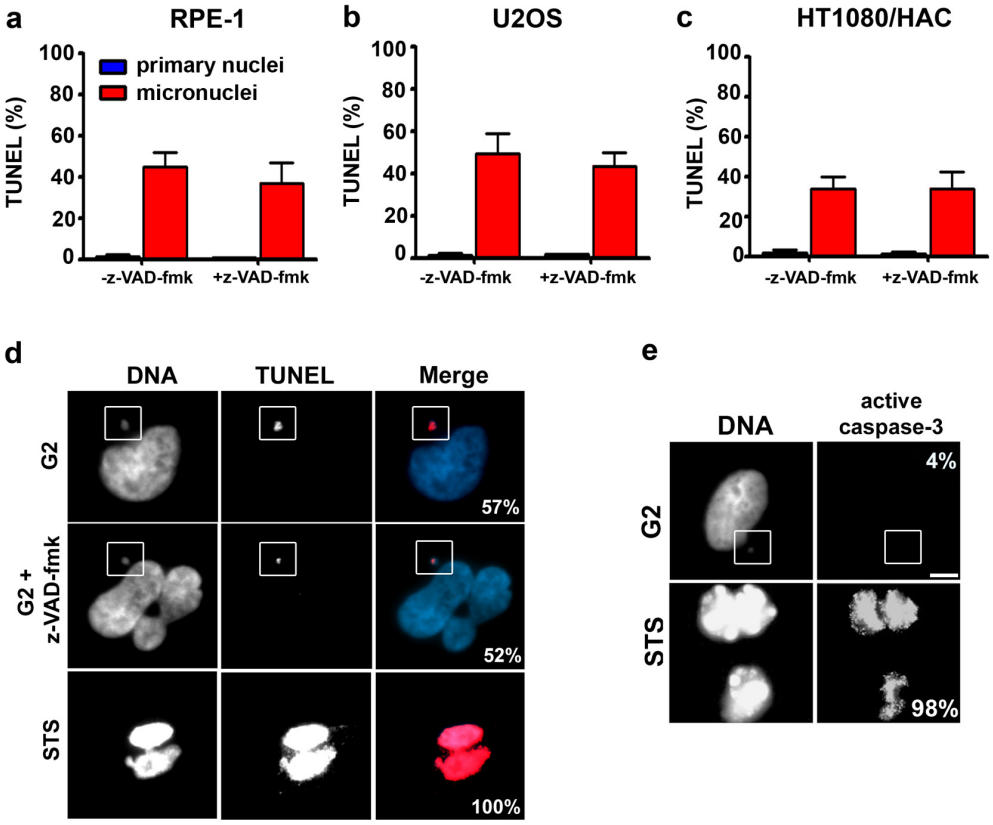

Supplementary Figure 5 (Related to Figures 1 and 2). Cells with DNA damage in micronuclei are not undergoing apoptosis. a-d, Treatment of cells with the pan caspase inhibitor z-VAD-fmk did not prevent TUNEL labeling of MN. (**a**) U2OS, (**b**) RPE-1 and (**c**) HAC-containing HT1080 cells were synchronized as in **Fig. 1, Fig. 2 and Supplementary Fig. 3** and released into media with 20 μM z-VAD-fmk or vehicle control. Cells were labeled for TUNEL at the G_2 timepoint. Data represent the means from three independent experiments ± SEM, n=100. Blue bars: primary nuclei; Red bars: MN. **d,** Representative images of U2OS cells from (**a**). Percentages indicate TUNEL-positive MN. 1 μM staurosporine (STS) is the positive control for induction of apoptosis. **e**, MN in G_2 cells do not contain active caspase-3. Cells released from nocodazole as in **Supplementary Fig. 3** were harvested at the G_2 timepoint and labeled to detect active caspase-3. Shown are representative images of cells with the percentages of cells labeling positive to detect active caspase-3 indicated in the upper right. (n=100 from each sample, two independent experiments). Scale bar, 10 μM.

Methods: For detection of active caspase-3 in (**e**), cells were incubated with the FITC-conjugated inhibitor DEVD-FMK (CASPGLOW fluorescein active caspase-3 kit) at a dilution of 1:300 at 37 °C for 1 h. DEVD-FMK binds irreversibly to activated caspase-3 in apoptotic cells.

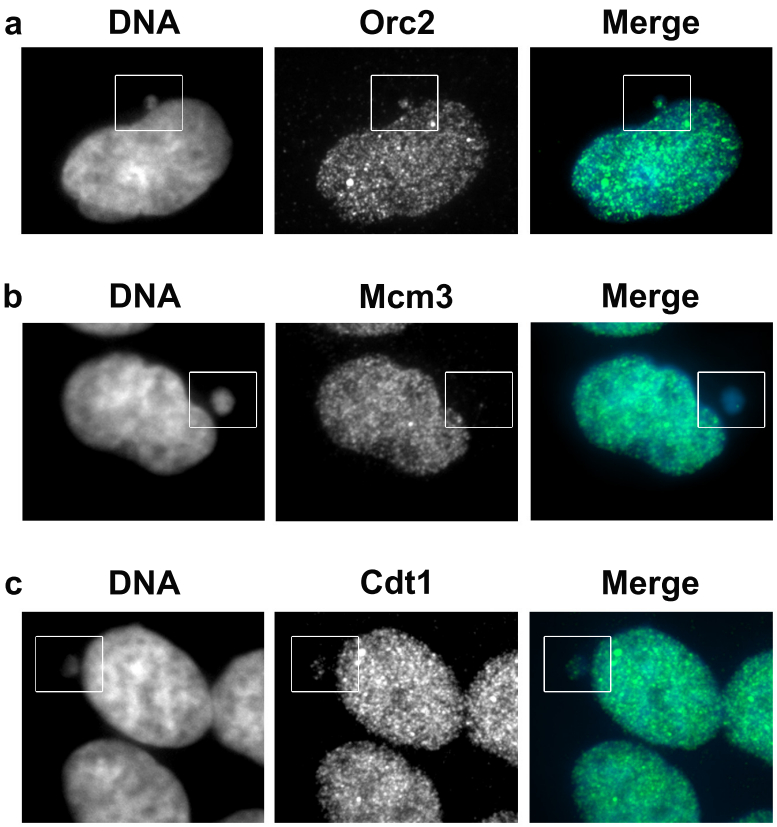

	Fluorescence Intensity Ratio (MN/PN)	
	DNA content	Area
a	0.931	0.957
b	0.022	0.018
c	0.254	0.309

Supplementary Figure 6 (Related to Figure 4). Mcm3 and Cdt1 recruitment is reduced in micronuclei, whereas Orc2 is recruited at normal levels. a-c, Representative images of MN-containing RPE-1 cells from the G_1 timepoint of protocol used as in **Fig. 1a**. Numbers indicate the mean ratio of fluorescence intensity of the indicated proteins in micronuclei relative to the signal in the primary nucleus. The fluorescence intensity of the replication proteins was normalized either to the DAPI fluorescence intensity or to the DNA area with similar results (n=100).

Discussion: The ORC complex and Cdt1 are required for loading of the DNA replicative helicase, MCM2-7 complex, when replication origins are licensed[49]. However this experiment suggests that the dramatic reduction of Mcm2 **(Fig. 4b)** and Mcm3 in MN cannot be explained by a defect in the recruitment of the ORC complex. Note that for detection of Orc2, Cdt1, Mcm2, and Mcm3, cells were preextracted with Triton-X100 to visualize chromatin bound protein. These findings are consistent with the fact that ORC loads rapidly and completely onto chromosomes in telophase, whereas only about 20% of MCM subunits load onto chromosomes in telophase, with the remainder imported gradually into the nucleus throughout G1[50]. Thus, the defect in MCM recruitment into MN is likely to be explained, at least in part, by nucleocytoplasmic transport defects in MN **(Fig. 4)**.

References:

(49) Arias, E.E. & Walter, J.C. Strength in numbers: preventing rereplication via multiple mechanisms in eukaryotic cells. Genes Dev 21, 497-518 (2007).
(50) Dimitrova, D.S., Prokhovora, T.A., Blow, J.J., Todorov, I.T. & Gilbert, D.M. Mammalian nuclei become licensed for DNA replication during late telophase. J Cell Sci 115, 51-59 (2002).

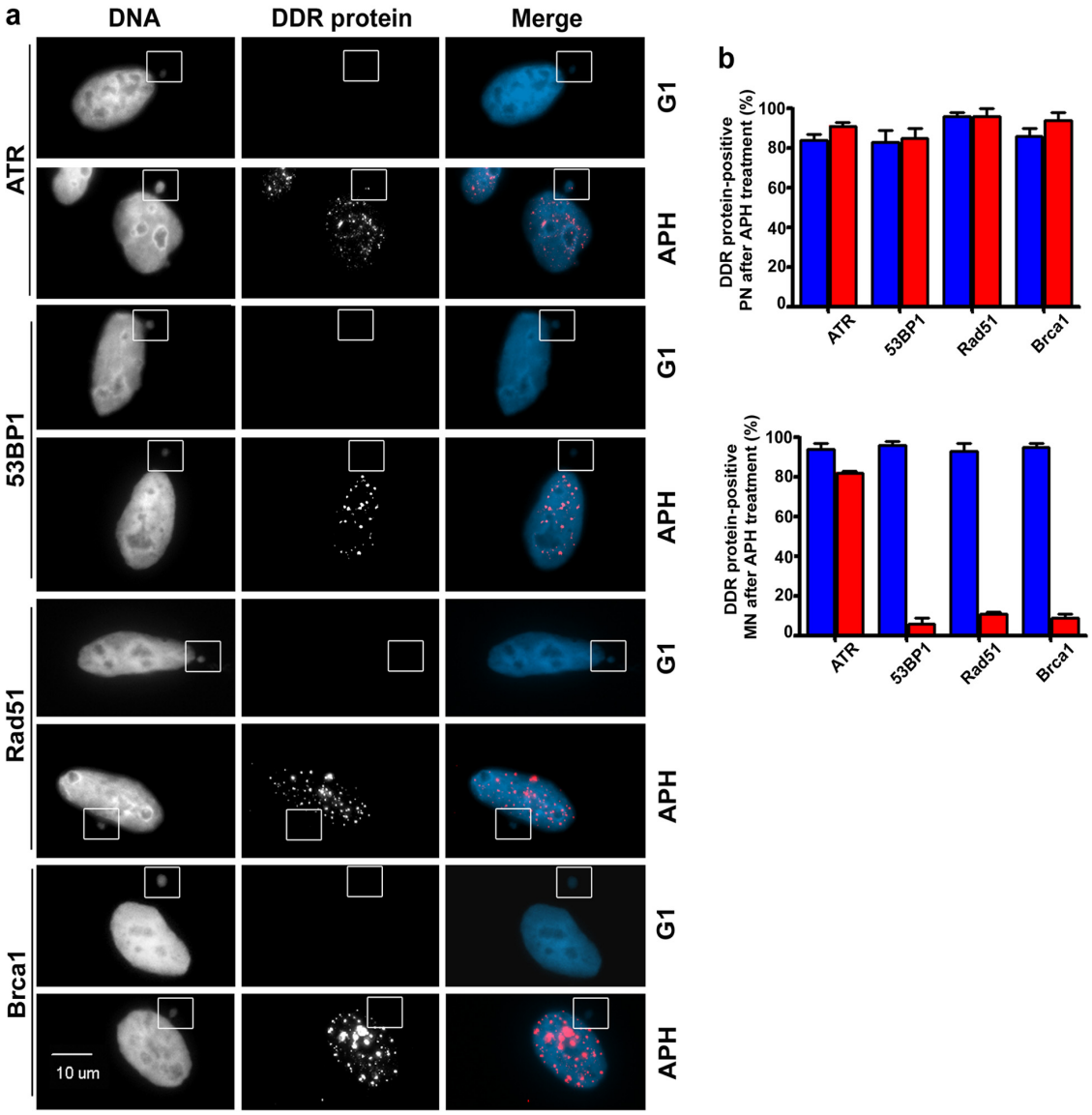

Supplementary Figure 7 (Related to Figure 4). Defective recruitment of DNA repair or DNA damage response (DDR) proteins into micronuclei upon DNA replication stress. (a) U2OS cells were released from a nocodazole block, exposed to 0.4 μM aphidicolin (APH) for 24 h or to a vehicle control, and stained for the indicated DDR protein. Shown are representative images of G_1 cells (negative control) and aphidicolin-treated (APH) cells. Scale bar, 10 μM. **(b)** Percentage of **(Top)** primary nuclei, PN and **(Bottom)** micronuclei, MN labelled with (Blue bars) γ-H2AX and (Red bars) DDR protein; n=100 for each sample. Data represents mean of two independent experiments ±s.e.m.

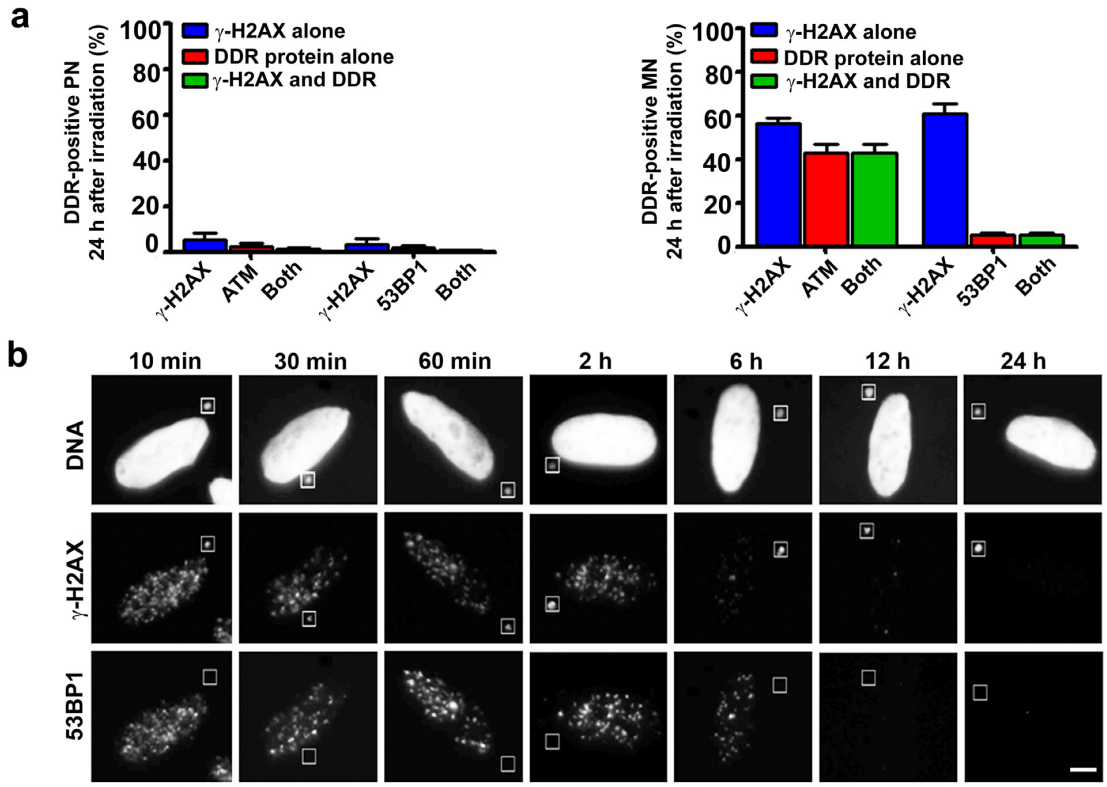

Supplementary Figure 8 (Related to Figure 4). Defective recruitment of DNA repair factors into micronuclei upon irradiation. **a**, Defective DNA damage response (DDR) in MN after IR. MN were induced in U2OS cells by the protocol in **Supplementary Fig. 2**. At the G_1 timepoint, cells were subjected to 2 Gy IR and collected at 24 h after IR. They were then labeled to detect the damage response factor, ATM or 53BP1. Percentage of (**Left)** primary nuclei, PN and **(Right)** micronuclei, MN labeled with Blue bars: for γ-H2AX alone; Red bars: for DNA damage response (DDR) proteins alone; Green bars: co-localization of γ-H2AX with the indicated DDR proteins (n=100 for each sample). Data represents mean of two independent experiments, ±SEM. **b**, 53BP1, the early participant in the DNA damage response (DDR), is not detected in MN after IR. Cells were treated as in **(a)**. Shown is co-localization of 53BP1 and γ-H2AX at indicated timepoints after IR. Scale bar, 5 μm.

Discussion: These data suggest that multiple aspects of the DDR response are defective in MN. This could synergize with the defect in MCM loading to produce chromosome breaks. Cells possess an excess of MCMs[51,52], but a reduction in MCMs reduces the density of replication origins, and, when combined with DNA damage, predisposes to genomic instability[53].

References:

(51) Ibarra, A., Schwob, E. & Mendez, J. Excess MCM proteins protect human cells from replicative stress by licensing backup origins of replication. Proc Natl Acad Sci 105, 8956-8951 (2008).
(52) Ge, X. Q., Jackson, D.A. & Blow, J.J. Dormant origins licensed by excess MCM2-7 are required for human cells to survive replicative stress. Genes Dev 21, 3331-3341 (2007).
(53) Kawabata, T. et al. Stalled fork rescue via dormant replication origins in unchallenged S phase promotes proper chromosome segregation and tumor suppression. Mol Cell 41, 543-553 (2011).

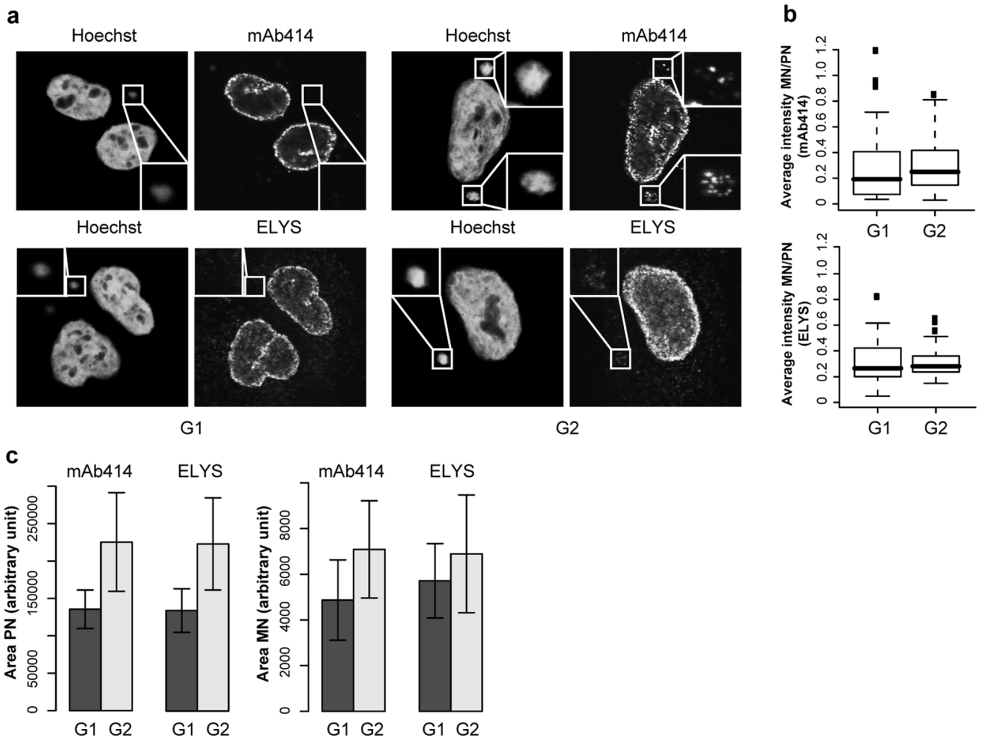

Supplementary Figure 9 (Related to Figure 4). Nuclear pore complex (NPC) assembly is defective in whole-chromosome micronuclei. a, Primary nuclei (PN) and MN of U2OS cells in G_1 and G_2 were stained for NPCs using mAb414 and ELYS antibodies. **b,** Quantitative analysis of NPC density. The ratio between the average fluorescence intensity of micronuclear and primary nuclear rim was calculated and illustrated as boxplots (mAb414: G_1, n = 34, median = 0.19; G_2, n = 35, median = 0.25; ELYS: G_1,n = 36, median = 0.26, G_2, n = 34, median = 0.28). Results were reproduced independently for mAb414 and ELYS (data not shown; mAb414: G_1, n = 25, median = 0.17, G_2, n = 38, median = 0.21; ELYS: G_1, n = 35, median = 0.39, G_2, n = 35, median = 0.41). **c,** PN and MN increase in size from G_1 to G_2. The area of PN and MN as determined by Hoechst staining was plotted (PN, mAb414: 1.7-fold; PN, ELYS: 1.5-fold; MN, mAb414: 1.5-fold; MN, ELYS: 1.2-fold).

Methods: MN were induced in U2OS cells by the protocol in **Supplementary Fig. 2**. At the respective timepoints, cells were pre-extracted for 5 min with PBS/0.5% Triton-X-100, fixed for 10 min with 4% paraformaldehyde, permeabilized for 5 min with PBS/0.25% Triton-X-100, and stained with mAb414 and ELYS antibodies.

Discussion: NPC density in MN is diminished 3.5-5-fold compared to PN both in G_1 and G_2. Therefore, the postmitotic pathway of nuclear pore assembly into the reforming nuclear envelope at the end of mitosis appears to be defective in MN. In addition to the postmitotic NPC assembly pathway, cells possess an interphase NPC assembly pathway allowing NPC assembly into the intact nuclear envelope and leading to doubling of the NPC number in growing interphase cells[54]. Beyond the expected increase in PN size (1.5-1.7-fold), we also saw a 1.2-1.5-fold increase in the size of MN. If the interphase NPC assembly pathway was defective in MN, one would expect a decrease in the ratio of NPC density in MN compared to PN from G_1 to G_2. However, the ratio of NPC density in MN/PN is constant or increases slightly from G_1 to G_2. This result suggests that the interphase NPC assembly pathway is not defective in MN.

References:

(54) Doucet, C.M,, Talamas, J.A. & Hetzer, M.W. Cell cycle-dependent differences in nuclear pore complex assembly in metazoa. Cell 141, 1030-1041 (2010).

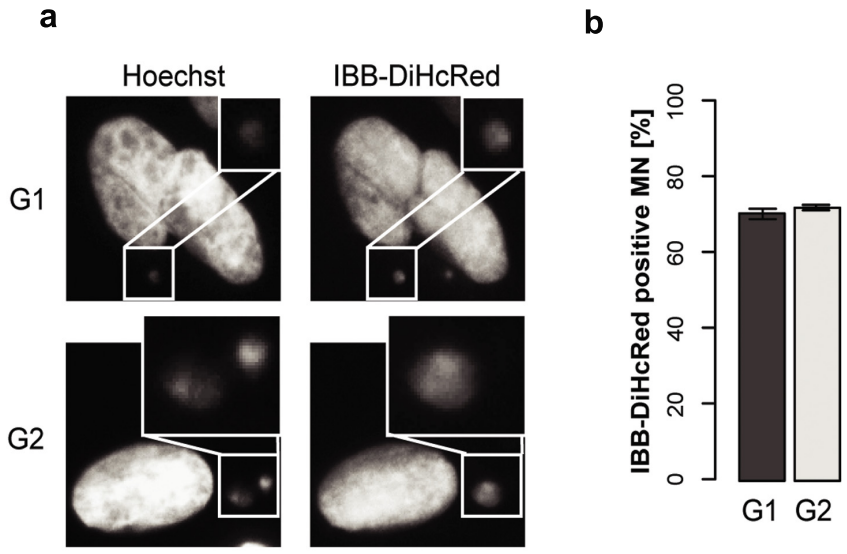

Supplementary Figure 10 (Related to Figure 4): Whole-chromosome micronuclei are partially defective for nuclear import of IBB-DiHcRed in G_1 and G_2. a, Representative images of micronucleated U2OS cells expressing IBB-DiHcRed in G_1 and G_2. **b,** Percentage of MN that show nuclear import of IBB-DiHcRed in G_1 and G_2 (Mean G_1: 70% +/- 2%; Mean G_2: 71.5% +/- 0.5%). Two independent experiments were performed and 100 micronucleated cells counted for each experiment.
Methods: U2OS cells were transiently transfected with IBB-DiHcRed-plasmid[55] and 24 h after transfection treated for 10h with 100 ng ml^{-1} nocodazole. Arrested mitotic cells were collected by mitotic shake-off and released into the cell cycle for 6 h (G_1) and 20 h (G_2). At the respective timepoints, cells were fixed for 10 min with 2% paraformaldehyde.

Discussion: The NFATc1-EGFP import assay **(Fig. 4c-d)** demonstrates that newly generated MN have a striking defect in nuclear import. However, this experiment demonstrates that over time (the G_1 sample is taken 6 h after the nocodozole release) significant import occurs in almost 70% of MN. This result is consistent with our finding that MN are not completely inert.

References:
(55) Dultz, E., Zanin, E., Wurzenberger, C., Braun, M., Rabut, G., Sironi, L. & Ellenberg, J. Systematic kinetic analysis of mitotic dis- and reassembly of the nuclear pore in living cells. J Cell Biol 180, 857-865 (2008).

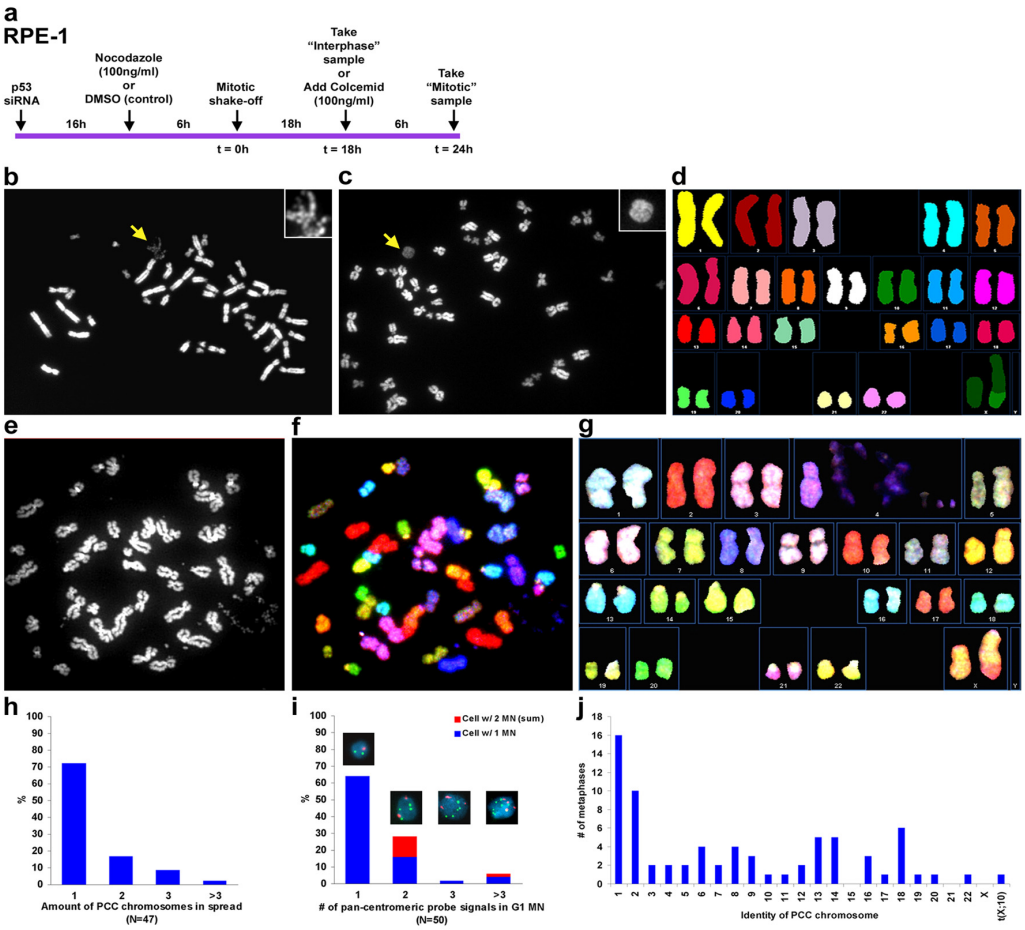

Supplementary Figure 11 (**Related to Figure 5**): **Cells with micronuclei exhibit chromosome pulverization**. **a**, Schematic representation of the experimental design. **b, c,** Representative metaphase spreads of cells harboring either a chromosome with PCC (**b**) or an intact MN (**c**) following nocodazole washout (yellow arrows; insets). **d**, Spectral karyotype (pseudo-colored) of a control RPE-1 cell. Note: The RPE-1 cell line is chromosomally stable with a modal chromosome number of 46; RPE-1 cells are female in origin and are known to have one karyotypically normal X-chromosome and one derivative X-chromosome with additional chromosomal material from chromosome 10 at the terminal end of the q-arm. **e-g**, An example of PCC in chromosome 4 from a single metaphase spread viewed with (**e**) DAPI staining (**f**) SKY probes (not pseudo-colored) and (**g**) as an aligned SKY karyotype. **h**, The percentage of metaphases with one, two, three, or more than three PCC chromosomes as determined by SKY. **i**, The percentage of interphase cells harboring one, two, three, or more than three chromosomes within single MN as determined by fluorescence in situ hybridization (insets: DNA (blue), pan-centromeric signals (red), pan-telomeric signals (green)); blue bars represent cells with one MN, red bars represent cells with two MN. **j**, The observed occurrence of PCC relative to chromosome identity.

Methods: MN were induced in RPE-1 cells as described in (**a**). Interphase cells (collected 18 h after nocodazole washout) and mitotic cells (collected 24 h after nocodazole washout) were resuspended in KCL for 18 min, fixed with Carnoy's solution, washed four times in Carnoy's fix, spread on slides and stained with Hoechst. Spectral karyotyping was performed as described in the Full Methods. For FISH, G_1 samples were collected at 6-8 h after nocodazole washout and fixed as above. Pan-centromeric probes (Cambio) and pan-telomeric probes (DAKO) were hybridized according to their respective manufacturers' protocols.

Discussion: We observe chromosome pulverization in cells with MN. The number of chromosomes pulverized during mitosis is highly correlated with the number of chromosomes initially observed in interphase MN (**h, i**). We note that chromosomes 1 and 2 exhibit elevated frequencies of pulverization (**j**).

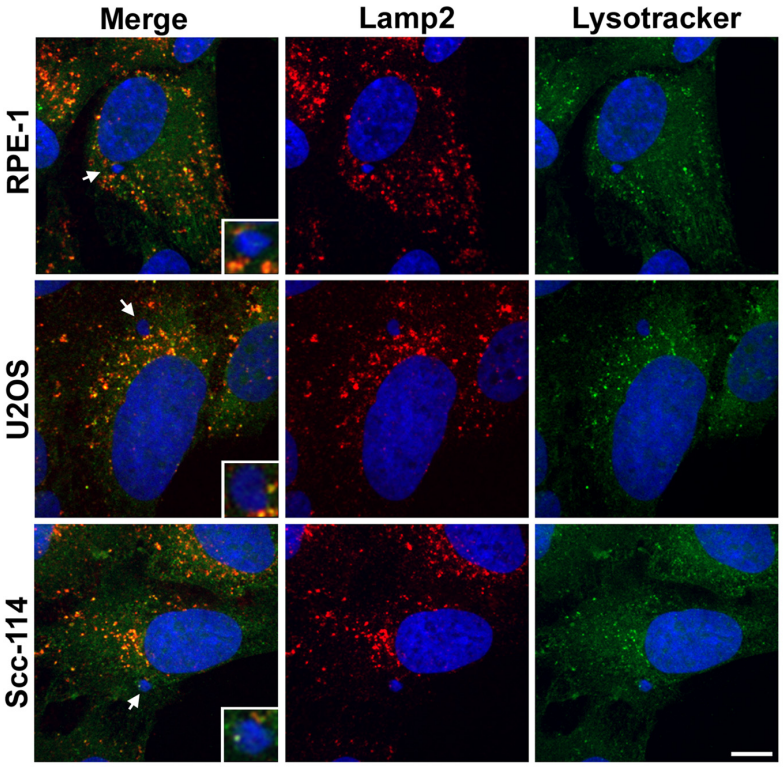

Supplementary Figure 12 (Related to Figure 5). Micronuclei do not associate with lysosomes. RPE-1, U2OS, and SCC-114 cells were stained for lysosomes (anti-Lamp2, red; Lysotracker, green) and DNA (Hoechst, blue). Spontaneously-arising MN (from U2OS and SCC-114 cells) as well as whole-chromosome MN induced by nocodazole-washout (from RPE-1 cells) were examined for co-localization with both lysosomal markers. In all cell lines, no conspicuous engulfment of MN by lysosomal markers was observed (insets, white). Results are from 3 independent experiments, n=75 MN for each cell line. Scale bar, 10 μM.

Methods:
To stain for lysosomes, cells were incubated with 50 nM Lystotracker (Invitrogen) for 1 h, rinsed in PBS, and then fixed in 4% paraformaldehyde for 10 min. Following fixation, cells were extracted in PBS-0.5% Triton X-100 for 5 min., blocked in TBS-BSA (10 mM Tris, pH 7.5, 150 mM NaCl, 5% BSA) for 30 min., and then incubated with Lamp2 primary antibodies (H4B4, Abcam) diluted at 1:200 in TBS-BSA for 30-60 min. After a 5-min wash in TBS-BSA, primary antibodies were detected using species-specific fluorescent secondary antibodies (Molecular Probes) and DNA was detected with 0.2 μg ml-1 DAPI (Sigma-Aldrich). Coverslips were mounted with ProLong Antifade mounting medium (Molecular Probes).

Cell Line	# MN Tracked	% MN Lost	# MN Tracked in Mitosis	% MN Reincorporated After Mitosis
HeLa (H2B-GFP)	56	5.4 %	51	9.8 %
Caco2 (H2B-GFP)	53	1.9 %	42	26.2 %
MDA-231 (H2B-mRFP)	53	15.1 %	38	0 %
SCC-114 (H2B-GFP)	78	2.6 %	59	18.6 %
SCC-114 (H2B-GFP) MCAK siRNA	28	0 %	18	27.8 %
U2OS (H2B-mRFP)	82	2.4 %	38	23.7 %
U2OS (H2B-mRFP) MCAK siRNA	106	0 %	44	6.8 %
U2OS-Kaede Nocodazole Washout	32	0 %	29	37.9%
U2OS (H2B-mRFP) Monastrol Washout	21	0 %	14	14.3 %
RPE-1 (H2B-mRFP)	5	0 %	3	33.3 %
RPE-1 (H2B-mRFP) MCAK siRNA	9	0 %	5	20.0 %
RPE-1 (H2B-mRFP) Nocodazole Washout	50	0 %	19	26.3 %

Supplementary Table 1. Micronuclei are stable and reincorporate with the primary nucleus during mitosis with appreciable frequency. Long-term live-cell imaging was used to determine the fate of spontaneously arising or experimentally induced (by MCAK siRNA, nocodazole washout, or monastrol washout) MN in a variety of cell lines. Micronuclei were identified as small (~1-5 nm in diameter), spherical, H2B-positive structures that were in approximately the same focal plane as the primary nucleus of the same cell. The total number of MN imaged (# MN Tracked) and the percentage that were lost from interphase cells during imaging (% MN Lost) are shown. Regardless of cell type, the vast majority of MN were stably maintained and visible until the onset of mitosis or the termination of filming up to 96 h later. Of the 16 MN lost during imaging, none were visibly degraded. While we cannot exclude the possibility that some of these MN were extruded from cells[61], it is far more likely that these MN were lost from view upon moving to just above or below the primary nucleus where they were rendered invisible. To estimate how frequently chromosomes in MN reincorporate with primary nuclei after mitosis, MN-containing cells were tracked through cell division. The total number of MN imaged through mitosis (# MN Tracked in Mitosis) and the percentage of cell divisions that gave rise to daughters that subsequently lacked MN (% MN Reincorporated After Mitosis) are shown.

References:

(61) Shimizu, N., Shimura, T. & Tanaka, T. Selective elimination of acentric double minutes from cancer cells through the extrusion of micronuclei. Mutat Res 448, 81-90 (2000).

Supplementary Movie Legends

Supplementary Movie 1. Live-cell imaging of a MN in a U2OS cell expressing H2B-mRFP. Upon mitosis, the chromosome within the MN fails to segregate into a daughter cell and thus reforms as a MN.

Supplementary Movie 2. Live-cell imaging of a MN in a U2OS cell expressing H2B-mRFP. Upon mitosis, the chromosome within the MN reincorporates into the primary nucleus of a daughter cell.

Supplementary Movie 3. Live-cell imaging of a MN in a U2OS cell expressing H2B-Kaede (corresponds to the cell shown in Figure 4g, top row). The MN is converted from emitting green fluorescence to emitting red fluorescence after activation with UV light. Upon mitosis, the chromosome within the MN segregates into a daughter cell and is reincorporated into the primary genome.

Supplementary Movie 4. Live-cell imaging of a MN in a U2OS cell expressing H2B-Kaede (cell is located in the bottom-left portion of the video and corresponds to the cell shown in Figure 4g, bottom row). The MN is converted from emitting green fluorescence to emitting red fluorescence by activation with UV light. Upon mitosis, the chromosome within the MN fails to efficiently segregate into a daughter cell and thus reforms as a MN. In the same video, an additional photo-converted MN can be observed to reincorporate into the primary nucleus of a daughter cell (top right portion of the video).